CIRP Journal of Manufacturing Science and Technology 37 (2022) 633–644

Contents lists available at ScienceDirect

CIRP Journal of Manufacturing Science and Technology

journal homepage: www.elsevier.com/locate/cirpj

Improvement of boring operations by means of mode coupling effect

Asier Astarloa[a,d,*], Alptunc Comak[b,c], Iker Mancisidor[a], Maria Helena Fernandes[d], Jokin Munoa[a,d], Zoltan Dombovari[e]

[a] Ideko – Member of BRTA, Dynamics & Control, Elgoibar, Basque Country, Spain
[b] Department of Mechanical Engineering, The University of British Columbia, Vancouver, BC V6T 1Z4, Canada
[c] Currently with MTU Aero Engines AG, 665 Dachauer Str., Munich 80995, Germany
[d] Mechanical Engineering Department, University of Basque Country (UPV-EHU), Bilbao, Basque Country, Spain
[e] Machine Tool Vibration Research Group, Department of Applied Mechanics, Budapest University of Technology and Economics (BME), Budapest, Hungary

ARTICLE INFO

Available online 4 April 2022

Keywords:
Chatter
Stability
Boring
RCSA
Mode coupling

ABSTRACT

Boring bars are inherently slender tools which are prone to show chatter problems due to their low dynamic stiffness and damping, being this problem their main limitation in productivity. The onset of chatter is mainly related to the dynamic stiffness of the bending mode of the boring bar when the length L to diameter D ratio is higher than 4. Tuned mass dampers (TMD) are effective technical solutions to increase the dynamic stiffness of large ratio boring bars. However, there are many applications where 4–6 L/D ratio tools are required, and the avoidance of chatter without the application of TMDs is interesting due to the high cost of damped tools. This work proposes the use of mode coupling effect to increase the damping and stabilise the machining process avoiding the use of any special device. This effect occurs when the frequency of one of the machine's modes is similar to the frequency of the dominant mode of the boring bar. As a result, the shape of the critical mode of the boring bar is mixed with the mode originated in the machine, and the damping and stability will be higher than the one that is not subjected to any dynamic coupling. The main contribution of this work is the application of this concept to increase stability in boring operations. This objective has been achieved by optimising the tool length and material by means of a dynamic model based on Receptance Coupling Substructure Analysis (RCSA). The model combines an analytical model of the elastic body of the boring bar with the experimental characterisation of the effect of the rest of the machine. This way, the shape and materials of the boring bar can be optimised to create an increase of damping. The optimisation procedure has been experimentally validated resulting in an increase of cutting stability and demonstrating that not always a shorter bar supposes a higher stability.

Introduction

In industry, internal machining operations are requested to produce parts like valves, bearing seats, long centre bores of shafts, pipes, engine cylinders and landing gears. The use of long slender tools named boring bars is required in all the internal operations. These cantilevered structures are prone to deflect and vibrate causing degradation in the produced surface quality. The lack of dynamic stiffness leads to self-excited vibrations known as chatter [1,2]. This type of vibration limits the productivity of the boring process, and in large length (L) to diameter (D) ratio holes ($L/D > 4$), makes the operation impossible to be accomplished [3].

Due to the limited effectivity of the process-based solutions, the increase of the cutting capacity of boring has been addressed mainly increasing the dynamic stiffness of the boring bar [4]. The topological optimisation of the boring bar cannot provide important improvements because the main geometrical parameters are fixed by the part. From the material point of view, high Young modulus materials like tungsten carbide have been used, but the stability improvement is not very high [5]. This problem was addressed by Rivin [3], suggesting a combined structure, which was made of carbide in the clamped part of the bar and aluminium in the free end. Graphite epoxy composite was selected by Lee and Suh [6], registering 5 times higher cutting capacity than a steel made boring bar.

The enhancement of the cutting capability of boring bars has been faced successfully by the introduction of tuned mass dampers (TMD) in the bars. Hahn introduced it for the first time for chatter

* Corresponding author at: Ideko – Member of BRTA, Dynamics & Control, Elgoibar, Basque Country, Spain.
E-mail address: aastarloa006@ikasle.ehu.eus (A. Astarloa).

https://doi.org/10.1016/j.cirpj.2022.03.008
1755-5817/

suppression in the middle of the 20th century [7]. This early version of damped boring bar based its working principle in the Lanchester damper, where a moving mass is connected to the structure only by a damping element. Donnies presented an improvement of this concept, adding a spring element [8]. Although Lanchester type dampers can dampen more than one mode [9], their efficiency is lower than a complete TMD [10]. This efficiency depends on the tuning of the mass, stiffness and damping [11]. Sims developed the optimal tuning formulation to maximise the stability against chatter [12]. While these dampers made use of viscous fluids and rubbers to introduce damping to the structure, dry friction-based dampers have also been developed [13]. A different approach was proposed by Matsubara, introducing piezo actuators in the base of the boring bar, where the strain energy is maximum. These piezo-actuators were connected to a LR circuit, which performs as a passive TMD [14].

Apart from these passive techniques, active damping has also been applied in boring bars. One of the first attempts was published by Glaser and Nachtigal based on a boring bar with two internal longitudinal hydraulic chambers [15] (in general terms, active or semi active approaches are based on devices located close to the tool tip or embedded in the base of the boring bar). Following this last approach, Tanaka et al. [16] placed piezoelectric actuators in the base of the bar, driving them with direct velocity feedback control algorithm. Electrorheological fluids have also been used in the base of the bars [17] to suppress chatter with stiffness and damping adjustment. Electromagnetic technology has also been applied to boring bars. Lu et al. [18] introduced this kind of actuator in two radial directions next to the base of the boring bar, introducing the force without contact for active damping of the bending modes. As a different approach, several authors have located inertial actuator close to the tool tip for chatter suppression. Tewani et al. [19] used piezo actuators to move an inertial mass, in parallel to the force flow, creating a counter force to dampen the vibration of the bar. Abele et al. based their active boring bar on a magnetic inertial actuator [20].

Regardless of their effectiveness, all these passive and active solutions require the development of a special tool with an embedded damper. Although the TMD equipped boring bars are an effective solution for large ($L/D > 7$) ratio boring bars, there are many applications in the stability limit, where 4–6 L/D ratio tools are used. In these cases, the avoidance of chatter without the use of tuned mass dampers is highly attractive for machinists due to the high additional cost of anti-vibration tooling. However, a different approach for the enhancement of the stability of boring processes using standard tools can be applied by taking advantage of the dynamic properties of the machine where the boring bar is attached. The idea is to select a boring bar in order to benefit from mode coupling phenomenon, creating a natural TMD without any additional device and maximising the dynamic stiffness of the critical mode. The application of this idea in the beforementioned overhang cases is the main contribution of this work.

When two structures with different modes are mechanically connected and their natural frequencies are similar, mode coupling occurs. Then, the working principle is similar to a TMD where the frequency of a controlled mode with high damping is tuned to be close to the frequency of the critical mode [21]. As a result, a new set of pair-modes is created mixing the shapes of the original modes and increasing damping. This concept, however, can be applied in different ways: while the TMD is an additional device attached to the structure in a parallel way in relation to the cutting force path, the mode coupling can also be applied in serial way inside cutting force flow without any additional device, by coupling the critical mode to an existing mode of the machine. This is an important point because the tuning process in serial configuration can reduce the cutting stiffness in the cutting point.

In the case of boring bars, as they are made in one single steel part, the damping of their bending mode is usually low. In addition, the turret of the lathe has its own vibration modes, and as the turret is composed by several parts which involves many interfaces, the damping value of these modes is relatively high [22]. Consequently, if mode coupling occurs, the dynamic response of the bending mode will be reduced, which in turn will increase the stability limit of the boring operations.

The use of the mode coupling effect to increase cutting capability was first studied by Duncan et al. [23] for high speed milling, verifying this effect experimentally. Houck et al. [24] developed a tuneable boring bar holder by using this effect to increase the dynamic stiffness of the tool. Schmitz et. al. proposed receptance coupling substructure analysis (RCSA) [25] to consider the interactions between tools with different lengths and machine dynamics. A similar approach was carried out by optimising the tail of a spindle [26] for milling purposes. Apart from these tool focused attempts, the mode coupling effect has also been used to increase the dynamic stiffness of parts by using a tuneable clamping table [21,27].

The main objective of this work is to use the mode coupling effect to increase the cutting stability without the need of any external damping device. To achieve this goal, the modelling of the dynamic flexibility of the combined machine/boring bar system by RCSA bar is considered in the second section. Later, the predictions of the dynamic model are verified experimentally. In the third section, the mode coupling effect is induced designing two different bars by using the length of the bar and different material distribution. Lastly, cutting tests are carried out clearly demonstrating the effect of mode coupling and the accuracy of theoretical description. As a result, it is proved that certain boring bar can have higher stability than a shorter boring bar.

Modelling of the receptance of the boring bar

The main objective of this subchapter is to predict the receptance or dynamic flexibility of the boring bar assembled on the machine, so that the presence of mode coupling effect can be estimated. The Frequency Response Function (FRF) in the tool tip is predicted by using a hybrid approach based on RCSA [25], which allows the coupling between experimental (machine side) and analytical (tool side) FRFs in order to obtain the resultant FRF at the tool tip. The present paper applies the methodology proposed by Park et al. [28] to experimentally characterise the stiffness and damping of the tool holder applying the inverse RCSA, and the method defined by Mancisidor et. al. [29] to predict the dynamics of the tools in free-free conditions based on the fixed boundaries approach for Timoshenko beams.

The complete assembly is divided in three substructures (see Fig. 1), including the machine with part of the interface between the tool and the turret (M), the boring bar body (B) and the boring head

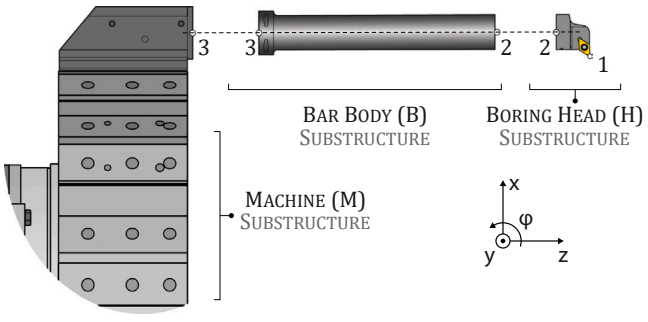

Fig. 1. Boring bar assembly is shown containing the machine (M) substructure, the bar body (B) substructure and the boring head (H). The parts connect at points 2 and 3, while the cutting edge is located at point 1.

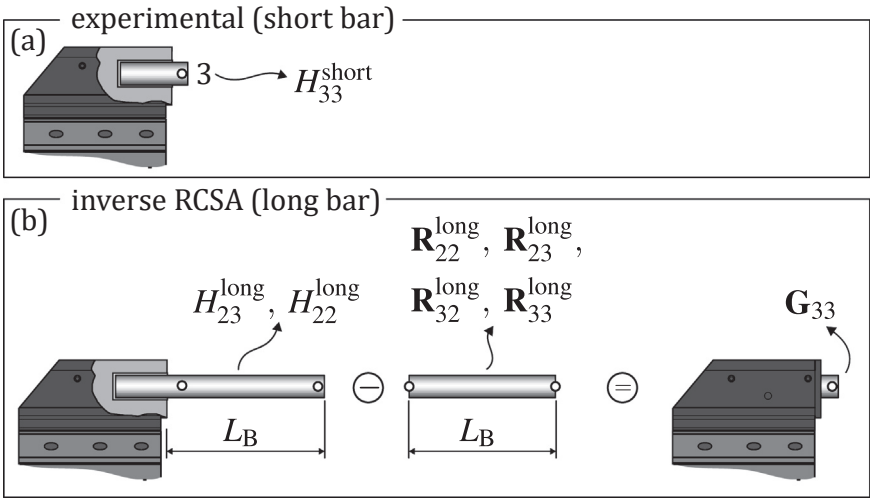

Fig. 2. represents the inverse substructuring to determine machine side (machine+interface, M+I) dynamics [28].

(H), whose effect in the final assembly cannot be neglected. The RCSA technique, based on Newton's laws, is then applied at two connection points, first at point 3 in order to couple machine and bar body substructures (Eq. (1)) and second at point 2 to assemble the result of the previous coupling ($\mathbf{G}_{22}$) with the boring head substructure (Eq. (2)):

$$\mathbf{G}_{22} = \mathbf{R}_{22} - \mathbf{R}_{23}(\mathbf{R}_{33} + \mathbf{G}_{33})^{-1}\mathbf{R}_{32}, \tag{1}$$

$$\mathbf{G}_{11} = \mathbf{R}_{11} - \mathbf{R}_{12}(\mathbf{R}_{22} + \mathbf{G}_{22})^{-1}\mathbf{R}_{21} \tag{2}$$

being $\mathbf{G}_{ij}$ the receptance matrices of an assembled structure between sensing point i and excitation point j, referred always to FRFs in the base on the machine, while $\mathbf{R}_{ij}$ are the theoretical receptance matrices of the substructure to be coupled obtained in free-free conditions. These receptances include translational and rotational degrees of freedom (see Eq. (3)), so that the wanted final translational receptance can be obtained as $H_{11} = G_{1x1x}$.

$$\mathbf{G}_{ij} = \begin{bmatrix} G_{ixix} & G_{ixi\varphi} \\ G_{i\varphi ix} & G_{i\varphi i\varphi} \end{bmatrix} \begin{pmatrix} \text{m/N} & \text{m/Nm} \\ \text{rad/N} & \text{rad/Nm} \end{pmatrix},$$

$$\mathbf{R}_{ij} = \begin{bmatrix} R_{ixix} & R_{ixi\varphi} \\ R_{i\varphi ix} & R_{i\varphi i\varphi} \end{bmatrix} \begin{pmatrix} \text{m/N} & \text{m/Nm} \\ \text{rad/N} & \text{rad/Nm} \end{pmatrix}. \tag{3}$$

RCSA technique requires to consider the additional structure at their connection points with free boundary conditions. Therefore, in order to estimate the final response of the boring bar assembly, first the obtention of machine receptance $\mathbf{G}_{33}$ and free-free response of the other two substructures are required. Next subchapters describe the achievement of these receptances.

Experimental modelling of the machine (G_{33})

In the present work, the machine (M) substructure is considered as a common base for all the predictions, so its receptance matrix $\mathbf{G}_{33}$ is obtained by means of experimental measurements. It could be also theoretically obtained, but considering that the prediction of the damping on the machine interfaces [30] is a difficult issue, the experimental characterisation of the dynamic response is an efficient approach to estimate the stiffness and the damping of the interface between the tool and the turret. The main problem is that the responses related to rotational degrees of freedom are not directly measurable. For that purpose, the method proposed by Park et al. [28] is used, wherein an inverse RCSA is applied over experimental FRFs obtained with a short and a longer "dummy" bars attached to the turret.

The method is based on three measurements (see Fig. 2): first, the direct translational transfer function with the short bar is experimentally measured, assuming that $G_{3x3x} = H_{33}^{short}$. After that, the direct and crossed translational FRFs with the long "dummy" bar (H_{22}^{long}, H_{23}^{long}) are experimentally measured, while the receptance matrices on the long bar in free-free conditions ($\mathbf{R}_{22}^{long}$, $\mathbf{R}_{23}^{long}$, $\mathbf{R}_{32}^{long}$, $\mathbf{R}_{33}^{long}$) can be calculated by employing either Finite Element Method (FEM) simulations or analytical beam theories (see subchapter 2.2). Then, by assuming that $G_{3x3\varphi} = G_{3\varphi 3x}$, RCSA technique can be inversely applied to obtain responses related to rotational degrees of freedom:

$$G_{3x3\varphi} = \frac{H_{23}^{long}(H_{33}^{short} + R_{3x3x}^{long})R_{2x3\varphi}^{long} - H_{23}^{long}R_{2x3x}^{long}R_{3x3\varphi}^{long} - H_{33}^{short}(R_{3x2x}^{long}R_{2x3\varphi}^{long} + (H_{22}^{long} - R_{2x2x}^{long})R_{3x3\varphi}^{long})}{H_{23}^{long}R_{2x3x}^{long} - R_{2x3x}^{long}R_{3x2x}^{long} + R_{3x3x}^{long}(R_{2x2x}^{long} - H_{22}^{long})}, \tag{4}$$

$$G_{3\varphi 3\varphi} = \frac{\begin{array}{l} G_{3x3\varphi}^2 R_{3x2x}^{long} - H_{33}^{short}R_{3x2x}^{long}R_{3\varphi 3\varphi}^{long} + H_{23}^{long}(H_{33}^{short} + R_{3x3x}^{long})R_{3\varphi 3\varphi}^{long} - G_{3x3\varphi}R_{3x3x}^{long}R_{3\varphi 2x}^{long} + H_{33}^{short}R_{3x3\varphi}^{long}R_{3\varphi 2x}^{long} \\ + G_{3x3\varphi}R_{3x2x}^{long}R_{3\varphi 2x}^{long} - H_{33}^{short}(G_{3x3\varphi} + R_{3x3\varphi}^{long})(G_{3x3\varphi} + R_{3\varphi 3x}^{long}) \end{array}}{H_{33}^{short}R_{3x2x}^{long} - H_{23}^{long}(H_{33}^{short} + R_{3x3x}^{long})}. \tag{5}$$

Dynamic modelling of the bar body (R_{22}, R_{23}, R_{33})

The application of the RCSA requires the estimation of the receptances of boring bar body in free-free conditions. Since the

objective of the work is to design a boring bar that meets the mode coupling effect, it requires to theoretically estimate its response before the bar body is manufactured. For that purpose, different methods can be applied. FEM simulations can be used, although complex modelling and meshing operations may hinder a quick dynamic response obtention. Alternatively, analytical beam theories such as Euler-Bernoulli's or Timoshenko's model can be applied.

The free-free receptances of the body of the boring bar can be directly calculated by the beam theories. However, the accurate prediction of the final receptance requires the calculation of a high number of modes. In this paper, the analytical approach proposed and validated by Mancisidor et al. [29] is adopted to overcome this drawback. It employs Timoshenko's beam theory in order to calculate the substructure response in fixed-free boundary conditions and the response is combined with fixed-boundaries method, adding the effect of rigid movements restrained in the fixed side. In this way, the benefits of Timoshenko's theory in front of other beam models are harnessed while the so-called cut-off frequency [31] of the Timoshenko beam model can be eluded, leading to well represented mode shapes for the final assembled model with the calculation of few modes.

Fig. 3 shows schematically the fixed boundaries approach, where the translation $\tilde{x}(t,z)$ and rotation $\tilde{\varphi}(t,z)$ of the free-free boundary conditions are calculated by the sum of the fixed-free responses $(x(t,z),\ \varphi(t,z))$ and the rigid body motion $\delta(t)$ and rotation $\vartheta(t)$ of the clamped side. Mathematically, it results as

$$\begin{aligned}\tilde{x}(t,z) &:= x(t,z) + \delta(t) - \vartheta(t)z = [1\ -z]\lambda(t) + \textstyle\sum_{k=1}^{n} U_k(z)q_k(t),\\ \tilde{\psi}(t,z) &:= \psi(t,z) + \vartheta(t) = [0\ -1]\lambda(t) + \textstyle\sum_{k=1}^{n} U_{\psi k}(z)q_k(t),\end{aligned} \tag{6}$$

being $\lambda(t) = [\delta(t)\ \vartheta(t)]^{\top}$, and $q_k(t)$ the modal displacements for the n number of modes calculated by Timoshenko's theory ([31,32]) for fixed-free boundary conditions, while $U_k(z)$ and $U_{\psi k}(z)$ are the mass normalised mode shapes related to deflection and angular motion, respectively. Then, according to [29], free-free condition modelled FRFs between an arbitrary excitation j and sensing i points can be calculated as

$$\mathbf{R}_{ij}(\omega) = \mathbf{T}_i \mathbf{Q}_c(\omega)\mathbf{T}_j^{\top}. \tag{7}$$

The transformation matrix and the core FRF are given as

$$\mathbf{T}_l = \begin{bmatrix} 1 & -z_l & \cdots & U_k(z_l) & \cdots \\ 0 & -1 & \cdots & U_{\psi k}(z_l) & \cdots \end{bmatrix},\ \mathbf{Q}_c(\omega) = \begin{bmatrix} -\omega^2 M_r & -\omega^2 M_c \\ -\omega^2 M_c^{\top} & -\omega^2 I + S_b \end{bmatrix}^{-1}, \tag{8}$$

where

$$\mathbf{M}_r = \rho A \begin{bmatrix} L_B & -\frac{1}{2}L_B^2 \\ -\frac{1}{2}L_B^2 & \frac{1}{3}L_B^3 \end{bmatrix},\ \mathbf{M}_c = \rho A \begin{bmatrix} \cdots & \int_0^{L_B} U_k(z)\mathrm{d}z & \cdots \\ \cdots & -\int_0^{L_B} U_k(z) z\ \mathrm{d}z & \cdots \end{bmatrix} \tag{9}$$

being , A and ρ the length, the cross section area and the density of the bar, respectively. Regarding the damping of the monolithic parts, it has been modelled as structural damping based on a constant loss factor η of the material, which is multiplied to a diagonal matrix containing the calculated natural frequencies ω_n:

$$\mathbf{S}_b(\omega) = (1 + \mathrm{i}\,\eta\ \mathrm{sgn}\ \ \omega)\mathrm{diag}\ \ \omega_{n,k}^2. \tag{10}$$

Numerical models based on finite element analysis (FEA) can be used to obtain the response of the boring bar as well, but the use of analytical formulae permits to accelerate the optimisation process described in section 4. The good correlation between Timoshenko beams compared to FEA models have been previously reported [29].

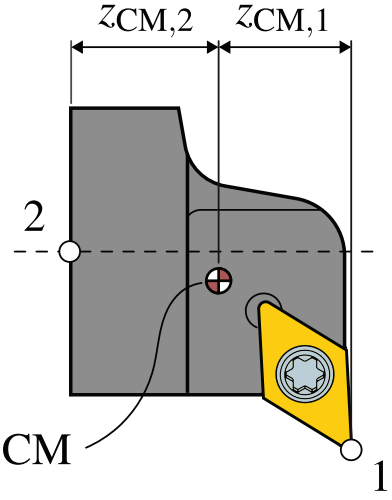

Fig. 4. Required input data for boring head modelling.

Modelling of the boring head (R_{11}, R_{12}, R_{22})

Due to the significant amount of mass and inertia of the head, this element cannot be neglected in the calculation of the response of point 1 (Fig. 1). This element acts like a linkage element between the boring bar body and the cutting insert, and it is interchangeable. Its bending can be neglected in the calculation, allowing its modelling as a rigid lumped mass element. (Fig. 4). Using analytical Newton-Euler equations to describe the translational and rotational inertial effects, free-free response between sensing point i and excitation point j point, characterised by their distance to the centre of mass (z_{CM}) can be formulated as:

$$\mathbf{R}_{i,j}(\omega) = -\frac{1}{\omega^2}\begin{bmatrix} \frac{1}{m_H} + \frac{z_{CM,i} z_{CM,j}}{\Theta_{CM}} & \frac{z_{CM,i}}{\Theta_{CM}} \\ \frac{z_{CM,j}}{\Theta_{CM}} & \frac{1}{\Theta_{CM}} \end{bmatrix}. \tag{11}$$

The rigid element is characterised by the mass m_H and the mass moment of inertia considered at the centre of mass (CM) ($\Theta_{CM,x}$ and $\Theta_{CM,y}$, accordingly to each of the bending directions). The values of

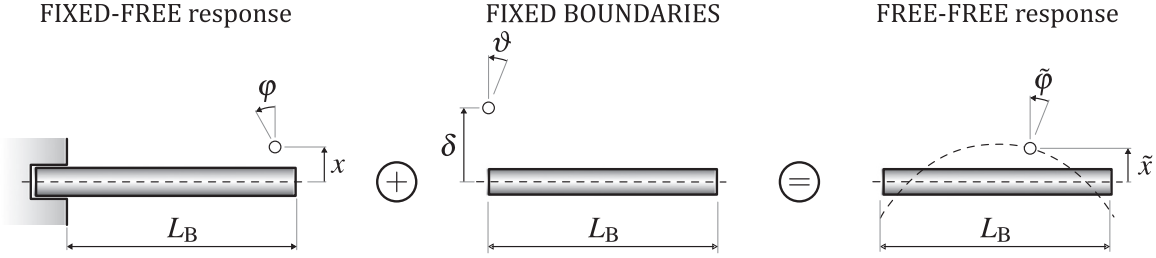

Fig. 3. Achievement of free-free boundary conditions response by adding clamped point movements to fixed-free boundary conditions response.

Table 1
Boring bar geometric and physical details.

D (mm)	d (mm)	ρ (kg/m^3)	E (GPa)	ν (1)	η (1)	L_{B2} (mm)	L_{B3} (mm)	m_H (kg)	$\Theta_{CM,x}$ (kgm^2)	$\Theta_{CM,y}$ (kgm^2)	$z_{CM,2}$ (mm)	$z_{CM,1}$ (mm)
50	6	7800	210	0.3	0.01	175	275	0.576	$1.94{\cdot}10^{-4}$	$1.85{\cdot}10^{-4}$	21	15

$\kappa = 6\frac{(1+\nu)(1+m^2)^2}{(7+6\nu)(1+m^2)^2+(20+12\nu)m^2} = 0.8541$, $m = \frac{d}{D}$ [31]

the mass and inertia of the different heads for the simulations are obtained from the CAD model provided by the manufacturer.

Experimental validation of the RCSA

In this subchapter, the analytical model used for the estimation of the FRF of the boring bar assembly is validated. For that purpose, H_{11} FRFs of two boring bars with different lengths (L_{B2}, L_{B3} in Table 1), including a boring head and mounted on a Danobat TCN12 horizontal lathe have been estimated and compared to experimental measurements.

The first step is to characterise the dynamic behaviour of the machine (M), composed by the machine itself, the turret and the Capto C5 tool interface. Following the work of [28], the combined dynamics can be semi-analytically determined as a function of frequency by measuring the direct translational receptance H_{33}^{short} of a short stub bar (L_{B1}=39 mm), and the direct H_{22}^{long} and cross H_{23}^{long} FRFs for a longer dummy bar (L_{B3}=275 mm) (see Fig. 2).

The measurements taken by impact testing presented in Fig. 5a clearly show on $H_{22}^{long}(\omega)$ and $H_{23}^{long}(\omega)$, that the first mode of the dummy bar L_{B3} is located at 346 Hz. The short stub bar L_{B1} does mostly have dynamics of the machine itself, so that $G_{3x3x}(\omega) = H_{33}^{short}(\omega)$ is justified. It can also be seen how significant the machine dynamic behaviour is, especially compared to a completely stiff (rigid coupling) situation. Moreover, Fig. 5a shows the turret modes of the lathe as dominant in x direction. The ~260 Hz and the ~390 Hz (T1&2 in Fig. 5a) modes are torsional modes of the turret structure roughly around its z axis creating relatively large lateral compliance at the tool connection point. These modes were separately confirmed with large scale modal analysis and are in the range to produce effective coupling with the tool modes.

Having defined the machine dynamics, two boring bars (L_{B2}, L_{B3}) have been modelled by using the method explained in section 2.2. The bars used for these tests are made from the same monolithic steel and they have the same cross section, with D as outer diameter and d as inner diameter. The related geometrical and physical data can be found in Table 1. Finally, a boring head with properties shown in Table 1 and geometry sketched in Fig. 4 have been analytically modelled and mounted on both bar cases.

An accurate prediction of the H_{11} receptances is observed in Fig. 6. Moreover, the effect of the dynamic behaviour of the machine is clearly visible in the experimental measurements due to the existence of modes which are coupled with the bending mode of the bars. It has been proved that the model is capable of estimating this coupled behaviour.

Design of dynamically coupled bars

The main objective of this work is to use the mode coupling effect to increase cutting stability. In the previous section, the model that allows an accurate prediction of the receptance at the tool tip has been developed. In this section, the model will be used to optimise the tool in order to promote the mode coupling effect. This optimisation can be done either by the modification of the tool length or the modification of the material of the tool. In both cases, the objective is to tune the natural frequency of the bending mode of the boring bar with the modes of the toolholder. In addition, a simple stability model has been used to validate the effect of

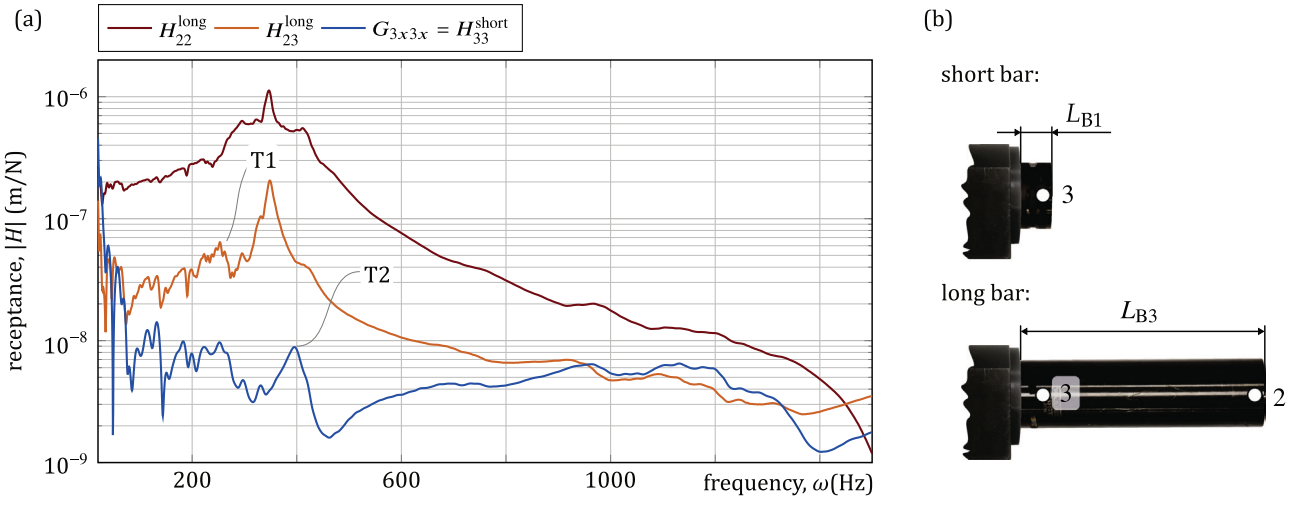

Fig. 5. *a)* shows the measured $H_{22}^{long}(\omega)$, $H_{23}^{long}(\omega)$, $H_{33}^{short}(\omega)$ and the determined $G_{3x3x}(\omega) = H_{33}^{short}(\omega)$, receptances in x direction. *b)* the short stub (L_{B1}=39 mm) and the long dummy (L_{B3}=275 mm) bars used for the method presented in [28].

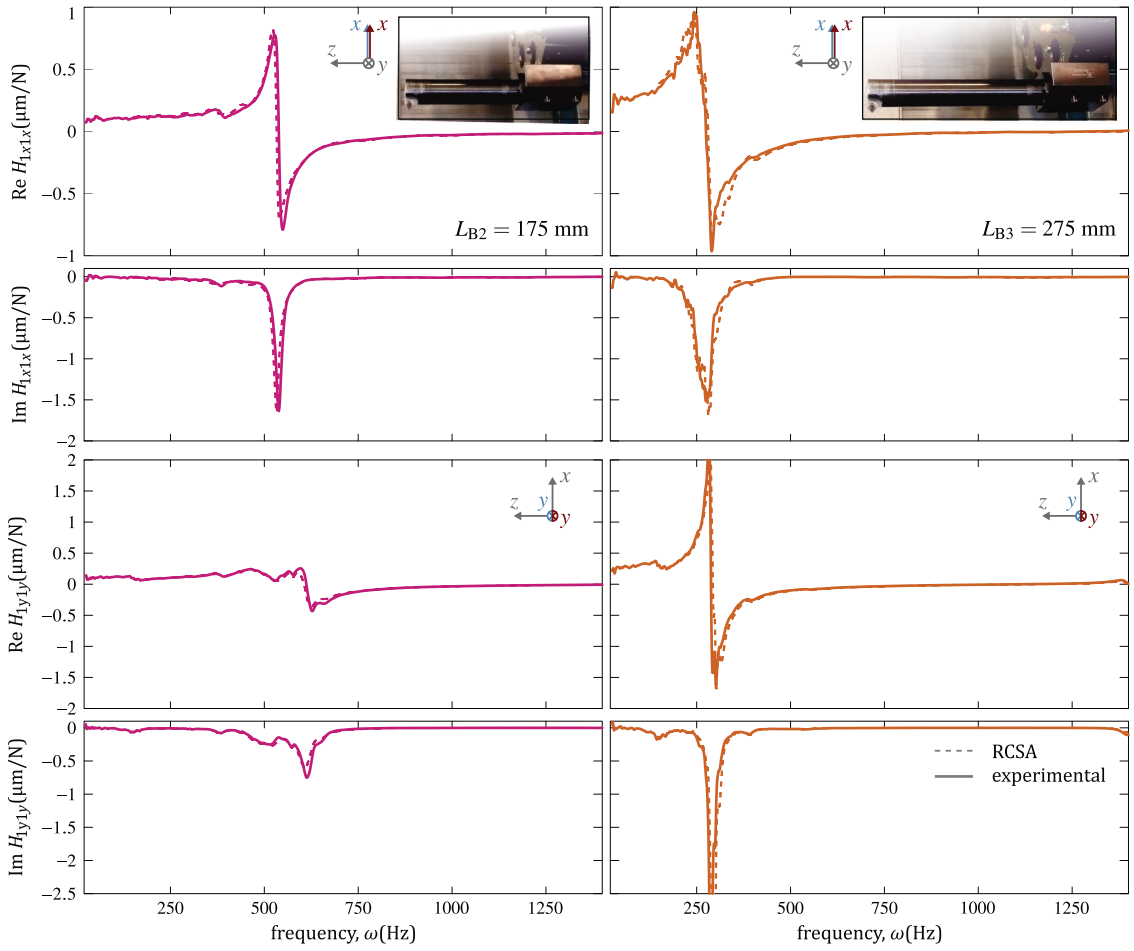

Fig. 6. Measured and predicted H_{11} FRFs in their real and imaginary parts in the two transversal directions (xy) for the two different boring bar assemblies (L_{B2}=175 mm and L_{B3}=275 mm).

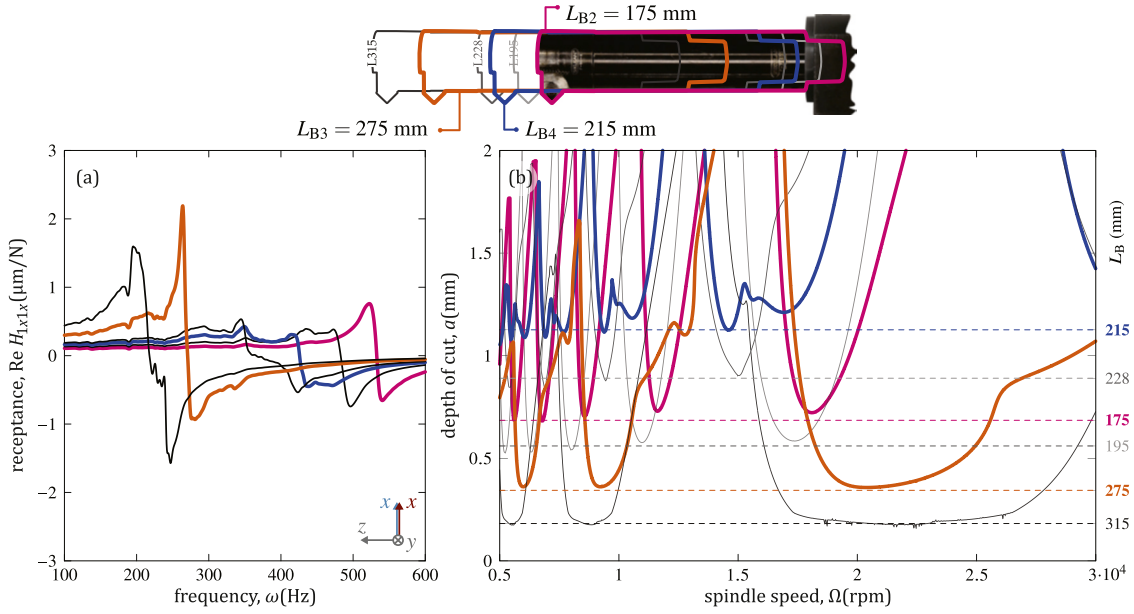

Fig. 7. *a)* shows the real parts of the simulated receptances $H_{11}$for different lengths in x direction; *b)* shows the stability lobes estimated from the simulated receptances for cutting conditions defined in Table 2.

Table 2
Tool and material data.

Workpiece material	AISI 1045 steel	
Cutting coefficients	$K_{c,t}$ (MPa)	1843
	$K_{c,r}$ (MPa)	625
	$K_{c,a}$ (MPa)	467
Tool	Insert	Sandvik SCMW 120408 5015
	κ (deg)	45
	r_e (mm)	0.8

different boring bars on cutting stability. A detailed explanation of this model can be found in the appendix.

Selection of the optimal length

With the same geometrical data as the one used in section 2.4, H_{11} FRFs of boring bar assemblies with boring bar lengths L_B from 175 to 315 mm have been estimated, being this overhang the unique change in the geometry of the bars.

Fig. 7a shows the real part of the simulated H_{11} receptances in x direction, which is the direction with the highest influence on the boring stability. The stability estimations for cutting conditions defined in Table 2 can be observed in Fig. 7b, calculated by means of the method defined in the appendix. The direct flexibility in the z direction and the effect of crossed receptances have not been considered in these simulations.

As expected, the stability model shows that the stability limit is broadly related to the minimum of the real part of the FRF, as shown in the literature [39]. Hence, the optimum length of the boring bar should be selected with this criterion. It can be observed that instead of showing higher flexibility as the overhang is increased, there are some overhangs where this trend is not followed due to the presence of mode coupling. When this happens, the logical rule of thumb that relates higher overhangs with lower stabilities is not fulfilled. Among the simulated options, L_{B4}:= 215 mm has been selected as the optimal length.

Material optimisation

The previous section it has shown that a higher overhang can result in a higher dynamic stiffness if mode coupling effect is present. However, under some circumstances the length of the boring bar cannot be modified. On the one hand, the length of the tool must be equal or larger than the length of the bore to be machined. On the other hand, the maximum length of the boring bar is limited by the machine's travelling distance and the length of the part. Hence, these restrictions limit the application of the variation of the overhang in the search of the mode coupling effect.

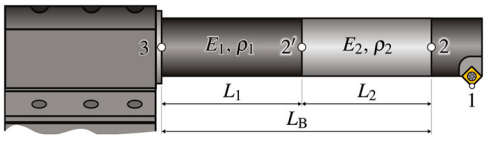

Fig. 8. Combined material boring bar assembly.

Table 3
Mechanical properties of combined boring bar body materials.

Material	**Young's modulus** (E)	**Density** (ρ)
Steel	210 Gpa	7800 kg/m^3
Aluminium	70 Gpa	2100 kg/m^3

The change of the boring bar's material allows the tuning of the frequency of the bending mode without varying the external geometrical dimensions of the bar. To validate this idea, a fixed boring bar length has been selected (L_B = 255 mm), dividing the boring bar body in two sections made of different materials. The bending frequency can be modified by the variation of the length of the sections, maintaining the total length of the bar. The model presented in section 2 is used, where 2 body bars are joined by RCSA (see Fig. 8). The mechanical properties of the selected materials are detailed in Table 3.

Fig. 9 shows the result of the material optimisation. It can be seen that the modification of the length of the segments allows a tuning of the frequency of the bending mode. The negative real part of the x direction receptance can be optimised for a combination of 225 mm of steel and 30 mm of aluminium thanks to the mode coupling (Fig. 9a). With this optimisation, a reduction of 50% is observed in the amplitude of the real part when compared to a full steel bar. Fig. 9b shows the stability estimations for cutting conditions defined in Table 2, where the benefit carried out by the optimal material combination is clearly observed.

Since aluminium section is located out of high strain energy area, its lower density affects more than the reduction of the stiffness, so that the natural frequency of the bar is increased with longer aluminium segments until a maximum value of L_2= 127 mm (Fig. 9c). For larger aluminium segments, the tendency is inverted resulting in a reduction of the natural frequency, and an important decrease of the static stiffness. The discontinuities on the natural frequency tendency show the mode coupling zone wherein the optimal aluminium length is selected (L_2=30 mm). In this zone, the static stiffness reduction is neglectable, being around 1% reduction for the selected optimal aluminium length (Fig. 9d).

Experimental validation

The present chapter aims to experimentally validate the mode coupling effect by measuring the benefit carried out by the optimal length boring bar estimated on subsection 3.1. For that purpose, the selected length (L_{B4}=215 mm) full steel boring bar has been manufactured and experimental measurements have been performed in order to demonstrate the improvement, both in the dynamic response of the system and in the stability of boring operations.

Experimental validation of the optimised bar dynamics

The manufactured boring bar (L_{B4}=215 mm), as well as the boring head, have been mounted in the TCN12 lathe and its dynamic responses have been experimentally obtained (see Fig. 10). The figure shows the comparison between the theoretical and experimental FRFs of the selected bar, which clearly proves that the model is able

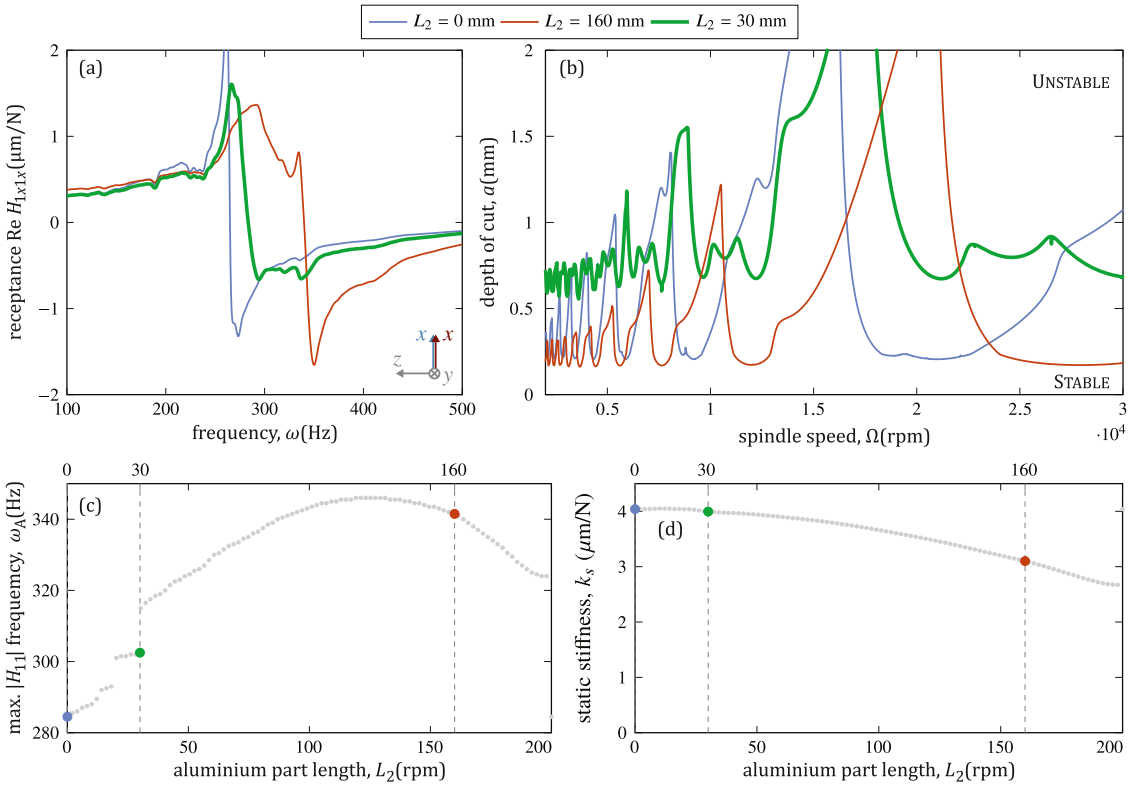

Fig. 9. *a)* shows the real parts of the simulated receptances $H_{11}$for different material combinations in *x* direction; *b)* shows the stability lobes estimated from the simulated receptances for cutting conditions defined in Table 2, *c)* shows the variation of the frequency corresponding to the highest amplitude of the FRF; *d)* shows the variation of the static stiffness.

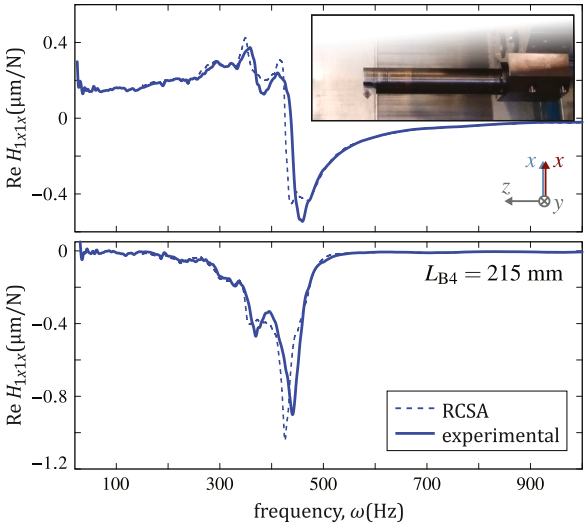

Fig. 10. Comparison of the dynamic response estimation in *x* direction for the cutting point and the experimental response for the optimised boring bar assembly in TCN12 lathe.

to predict the combined dynamics of the boring bar machine tool assembly.

In the *x* direction, which is the most important as it modifies the chip width, hence affecting the stability, the selected bar (L_{B4}) presents significantly less flexibility than the other two bars (L_{B2}, L_{B3}), which should result in higher cutting stability. Neither the short bar L_{B2} (inconsistently) nor the long bar L_{B3} (unnaturally) can overcome the dynamic stiffness of the selected bar (see Fig. 6).

Effect of the machine on the mode coupling

As the mode coupling is a phenomenon where the resulting FRF depends of both tool and machine dynamic behaviour, selected bar length assembly, in addition to the short (L_{B2}=175 mm) and long (L_{B3}=275 mm) bar assemblies have been mounted in 2 additional clampings: the turret of a different lathe (Danobat NI750) and a heavy duty milling machine bed. This last clamping consists of a 6-metre-long cast iron bed, which has no vibration modes in the frequency range of the bending modes of the bars, resulting in a very stiff clamping without any mode interaction effect.

Predicted mode coupling effect has been proven for a bar selected by RCSA estimations (Fig. 6 & Fig. 10) based on the dynamic behaviour of TCN12 lathe. However, the change of the machine substructure (M) can completely modify the response of the assembly.

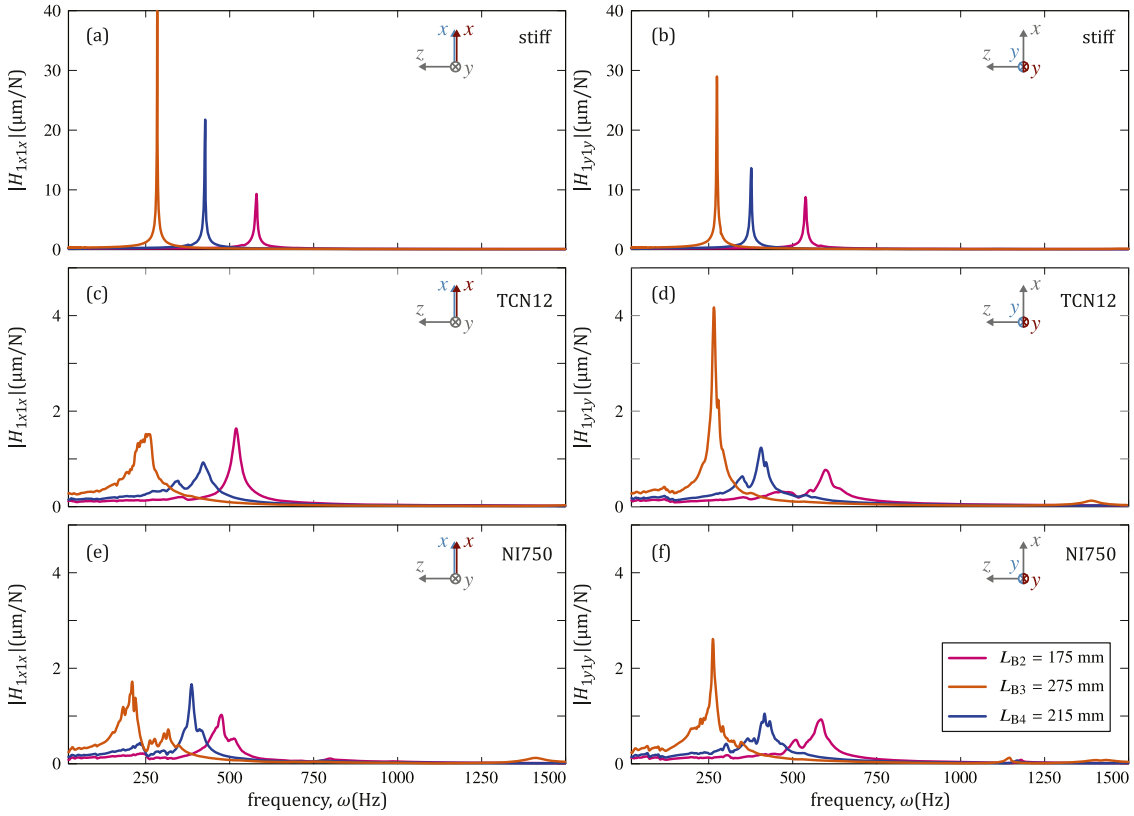

Fig. 11. FRFs of the boring bar assemblies in different clampings. In *a) & b)* bars were measured in a dynamically stiff milling machine bed. In *c) & d)* measurement comparisons are presented for bars mounted in TCN12 lathe, while in *e) & f)* the same are shown for NI750 lathe.

Table 4
Cutting conditions.

Spindle speed (rpm)	250, 460 and 620
Cutting speed (m/min)	~ 120
Feed (mm/rev)	0.15
Depth of cut (mm)	0.2–3

Indeed, the stiff clamping made in the milling machine bed shows (Fig. 11a & Fig. 11b) the trend where the dynamic stiffness and the natural frequency are reduced as the overhang is increased. This expected behaviour occurs due to the absence of interaction with the modes of the clamping structure.

In the case of NI750 lathe (Fig. 11e & Fig. 11f), the mode coupling effect is present, but as this lathe has a different dynamic behaviour from the TCN12 one, the optimal bar length is different. Therefore, the optimal boring bar length calculated in subsection 3.1 is only valid for the TCN12 lathe.

Cutting tests

Finally the stability is verified by means of cutting tests performed in three different spindle speeds (Table 4) by using the three boring bar assemblies proposed in the previous chapter (L_{B2}, L_{B3}, L_{B4}) in the TCN-12 lathe.

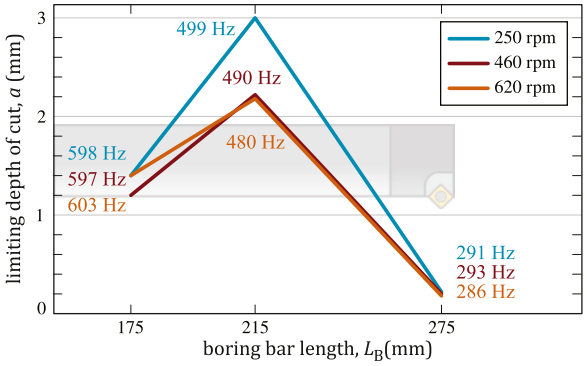

Fig. 12. Limit depth of cut and chatter frequency obtained from experimental cutting tests for the three boring bar lengths.

As shown in Fig. 12, experimental cutting tests show a significant stability improvement when the coupled bar L_{B4} is used, while the shortest bar L_{B3} offers lower stability despite its shorter overhang. Specifically, the stability limit is almost doubled although the bar length is increased by 23%. Finally, the longest bar L_{B2} undergoes significant decline in stability as it was expected and the bar was not able to perform stable cuts in any tried depth of cuts. The chatter

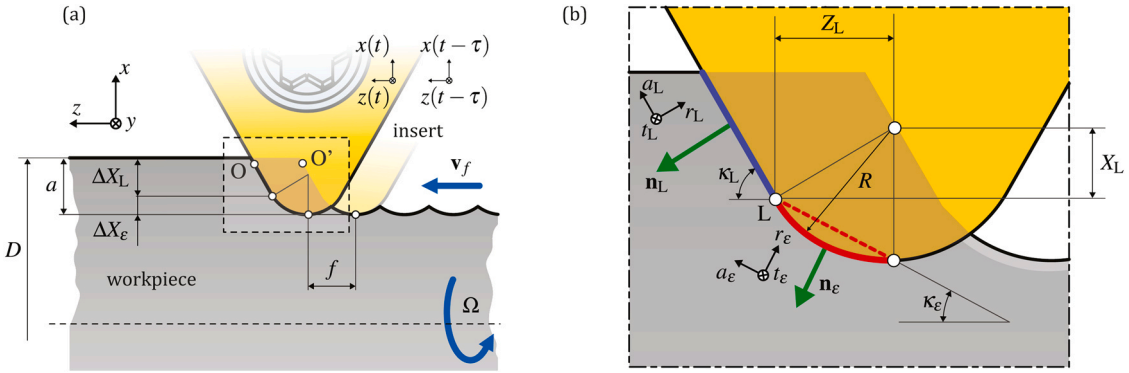

Fig. 13. *a)* The sketch of simple chamfered wedge like geometry turning model; *b)* detailed view of the geometry, where the nose radius part ε (red) and linear edge part L (blue) can be differentiated.

frequencies match with the main critical mode frequencies measured for each of the bars (see Fig. 6 & Fig. 10).

The results prove that the linearity between bar overhang and stability limit can be broken by the mode coupling effect. Therefore mode coupling technique is demonstrated as a quite counter-intuitive possibility to attenuate vibration for boring bars, by systematically finding a length where coupling can be established, without the significant expected decline of stability.

Conclusions

The dynamic behaviour of the turret/machine side has an important role in the boring bar dynamics. It has been proven both analytically and experimentally that mode coupling affects beneficially to the dynamic behaviour of the boring bars increasing the damping and the cutting capability. This way the use of tuned mass dampers can be avoided, resulting in an economic and efficient solution in shop floor environment for boring bars with slenderness (L/D) below 7.

In workshop environment, the selection of the length of a boring bar is subjected to the depth of the hole to be bored, choosing the shortest possible overhang. However, the present paper demonstrates that an improvement of machining stability can be achieved taking into consideration the machine side's dynamic behaviour in the selection of the bar length, which may involve a higher overhang than the geometrically needed one or a combination of different materials in the boring bar.

With the presented RCSA based technique, the dynamic behaviour of the turret can be characterised, and the effect of different bars can be simulated. On the one hand, resulting model has been used to calculate the optimal boring bar length which have been validated experimentally. On the other hand, the model can also be used for a combination of materials in the manufacturing of the bar in order to have mode coupling effect without varying the total tool overhang.

Experimental measurements and cutting tests demonstrate that the calculated optimal length bar does not only have better behaviour than the longer one, but it also has performed better than the shorter one, due to the mode coupling effect.

Appendix

Stability of boring operation.

Although the model presented in section 2 is capable of predicting FRFs, a stability model has been used to estimate the effect of different boring bars on cutting stability. Since boring operation usually corresponds to operations with large ratio between chatter frequency and tooth passing frequency, the process can be greatly affected by the process damping effect [33–35]. However, considering that the stability prediction is not the purpose of the present paper and given the complexities of accurate turning stability model, the authors propose to use a simple regenerative model of turning operation [1,10] to compare relatively the effect of the mode coupling in the optimisation process (section 4).

The edge geometry is simply considered as a wedge like geometry (Fig. 13), with a chamfer for modelling the average effect of nose radius (R).

A linear force model [36] has been used with local tangential (t), radial (r) and axial (a) coordinate system, defined as

$$\mathrm{d}\mathbf{F}_{tra}(h) = (\mathbf{K}_e + \mathbf{K}_c h)\mathrm{d}s,$$

where $\mathbf{K}_e$ and $\mathbf{K}_c$ contain the edge and cutting coefficients in *tra* system, respectively. In (12), h is the local chip thickness defined approximately between two successive turns (O′→O) and in order to calculate it, the insert is split into the nose radius part and the linear wedge part ($j = \varepsilon, L$) (see Fig. 13-b) extending the classical model of Colwell [37]. The effect of the nose radius is considered with an average lead angle (chamfer) $\kappa_\varepsilon = \kappa_\varepsilon(a)$ calculated depending on the used depth of cut (wedge-chamfer). The tangent point L in Fig. 13 can be determined to the centre point of the edge radius as

$$X_L = -R\cos\kappa_L, \quad Z_L = \begin{cases} R\sin\kappa_L, & \kappa_L \neq \pi/2, \\ R, & \kappa_L = \pi/2, \end{cases} \tag{13}$$

The different involvement of the edge segments is determined as follows

$$\Delta X_L = \max\{a - R - X_L, 0\} \quad \text{and} \quad \Delta X_\varepsilon = \min\{a,\ R + X_L\}. \tag{14}$$

Then, considering simple geometry, the lead angle of the edge-radius-chord (chamfer) can be determined as

$$\kappa_\varepsilon = \arctan\frac{R + X_L}{Z_L}. \tag{15}$$

Knowing the lead angles on both parts, the chip thickness can be defined for its part with projection in chip thickness direction ($\mathbf{n}_j = [-\cos\kappa_j\ 0\ \sin\kappa_j]^T$) as

$$h_j(t) = (f + \Delta\mathbf{r}(t))\mathbf{n}_j, \tag{16}$$

where f is the feed per revolution ($f = v_f\tau$) and $\Delta\mathbf{r}(t) = \mathbf{r}(t) - \mathbf{r}(t-\tau)$, being $\mathbf{r}$ the vibration movement in xyz coordinate system ($\mathbf{r}(t) = [x(t)\,y(t)\,z(t)]^T$) and τ the regenerative delay related to the angular velocity of the workpiece ($\tau = 2\pi/\Omega$). By avoiding the strict derivation, the force is in xyz

$$\mathbf{F}_{xyz}(t) = \sum_{j=\varepsilon,L} \mathbf{T}_j \frac{\Delta X_j}{\sin\kappa_j}(\mathbf{K}_e + \mathbf{K}_c \otimes\ \mathbf{n}_j\Delta\mathbf{r}(t) + \mathbf{K}_c f\ \sin\kappa_j), \tag{17}$$

where $\mathbf{T}_j$ is the transformation matrix between *tra* and *xyz* coordinate systems:

$$\mathrm{T}_j = \begin{bmatrix} 0 & \cos\kappa_j & \sin\kappa_j \\ 1 & 0 & 0 \\ 0 & \sin\kappa_j & \cos\kappa_j \end{bmatrix}. \tag{18}$$

Then, dynamic behaviour of the boring bar can be described in Cartesian coordinates, where M, C and K are the mass, damping and stiffness matrices, respectively, while modal transformation can be performed by using mass normalised modal transformation matrix **U**.

$$\mathbf{M}\,\ddot{\mathbf{r}}(t) + \mathbf{C}\,\dot{\mathbf{r}}(t) + \mathbf{K}\,\mathbf{r}(t) = \mathbf{F}_{xyz}(t, \mathbf{r}(t), \mathbf{r}(t-\tau)), \tag{19}$$

$$\mathbf{U}^{\top}\mathbf{M}\,\mathbf{U}\,\ddot{\mathbf{q}}(t) + \mathbf{U}^{\top}\mathbf{C}\mathbf{U}\,\dot{\mathbf{q}}(t) + \mathbf{U}^{\top}\mathbf{K}\mathbf{U}\,\mathbf{q}(t) = \mathbf{U}^{\top}\mathbf{F}_{xyz}(t,\ \mathbf{q}(t),\ \mathbf{q}(t-\tau)). \tag{20}$$

Assuming the proportional damping, the matrix valued equation of the left-hand-side is diagonalised and decoupled, considering $\mathbf{U}_i$ as the column of the modal vector matrix related to each mode ($i = 1, 2, \ldots, n$).

$$\ddot{q}_i(t) + 2\zeta_i\omega_{\mathrm{n},i}\dot{q}_i(t) + \omega_{\mathrm{n},i}^2 q_i(t) = \mathbf{U}_i^{\mathrm{T}}\mathbf{F}_{xyz}(t, \mathbf{q}(t), \mathbf{q}(t-\tau)), \tag{21}$$

where the modal parameters can be obtained from the final translational receptance H_{11}. This kind of equations can be analysed either by semidiscretization [38] or Nyquist method [33]. In our case, semidiscretization method has been used where the discretized counterpart of the solution operator (step matrix) is derived, and if the stability is ensured if all eigenvalues of the step matrix have their magnitude less than unity.

Concerning the modal parameters, in a usual situation, the boring bar has a clear dominant mode related to the bending/rotation of the bar. Therefore, it is easy to perform a curve fitting and obtain modal parameters for the application of the semi-discretization method. In this situation, manual fittings such as Rational Fraction Polynomials (RFP) [39] or Polyreference [40] can be applied efficiently.

However, when mode coupling happens, two modes are really close and the accurate extraction of the modal parameters can be complex. In order to simplify the process, this work employs the so-called Impulse Dynamic Subspace (IDS)[41].

In addition, although vibrations in both *x* and *z* directions can have influence on the stability, in the present paper only *x* direction is considered given the considerably higher flexibility of boring bars in this direction.

Declaration of Competing Interest

The authors declare that they have no known competing financial interests or personal relationships that could have appeared to influence the work reported in this paper.

Acknowledgements

The authors thank the collaboration of Markel Sanz from IDEKO. This work has been supported by EUROSTARS FORTH E!12998 project and the EU Horizon 2020 InterQ project (958357/H2020-EU.2.1.5.1).

References

[1] Tlusty, J., Polacek, M., 1957, Beispiele der behandlung der serlbsterregten schwingung der werkzeugmaschinen. Hanser Verlag, Munich. 3rd FoKoMa.
[2] Tobias, S.A., Fishwick, W., 1958, Theory of Regenerative Machine Tool Chatter. The Engineer, 205.
[3] Rivin, E.I., Kang, H., 1992, Enhancement of Dynamic Stability of Cantilever Tooling Structures. International Journal of Machine Tools and Manufacture, 32/4: 539–561. https://doi.org/10.1016/0890-6955(92)90044-H.
[4] Munoa, J., Beudaert, X., Dombovari, Z., Altintas, Y., Budak, E., Brecher, C., Stepan, G., 2016, Chatter Suppression Techniques in Metal Cutting. CIRP Annals, 65/2: 785–808. https://doi.org/10.1016/j.cirp.2016.06.004.
[5] Mannan, M.A., Lindström, B., 1986, Performance for End Mills Made of Different Tool Materials with Regards to Tool Life and Stability. CIRP Annals, 35/1: 37–40.
[6] Lee, D.G., Suh, N.P., 1988, Manufacturing and Testing of Chatter Free Boring Bars. CIRP Annals, 37/1: 365–368. https://doi.org/10.1016/S0007-8506(07)61655-2.
[7] Hahn, R.S., 1951, Design of Lanchester Damper for Elimination of Metal Cutting Chatter. Transactions of the ASME, 73:331.
[8] Donies J., Van der Noortgate L., 1974. Alesage Des Trous Profonds Sans Broutage (in English: Boring out of deep holes without chatter). CRIF Note Techn:33.
[9] Yang, Y., Xu, D., Liu, Q., 2015, Milling Vibration Attenuation by Eddy Current Damping. The International Journal of Advanced Manufacturing Technology, 81/1: 445–454. https://doi.org/10.1007/s00170-015-7239-3.
[10] Tobias, S.A., 1965, Machine-tool Vibration. Blackie & Sons Ltd, London.
[11] Den Hartog, J., 1934, Mechanical Vibrations. McGraw-Hill Book Company, New York/London.
[12] Sims, N.D., 2007, Vibration Absorbers for Chatter Suppression: A New Analytical Tuning Methodology. Journal of Sound and Vibration, 301/3–5: 592–607. https://doi.org/10.1016/J.JSV.2006.10.020.
[13] Ema, S., Marui, E., 1996, Damping Characteristics of An Impact Damper and its Application. International Journal of Machine Tools and Manufacture, 36/3: 293–306. https://doi.org/10.1016/0890-6955(95)00073-9.
[14] Matsubara, A., Maeda, M., Yamaji, I., 2014, Vibration Suppression of Boring Bar by Piezoelectric Actuators and LR Circuit. CIRP Annals, 63/1: 373–376. https://doi.org/10.1016/J.CIRP.2014.03.132.
[15] Glaser, D.J., Nachtigal, C.L., 1979, Development of a Hydraulic Chambered, Actively Controlled Boring Bar. Journal of Engineering for Industry, 101/3: 362. https://doi.org/10.1115/1.3439519.
[16] Tanaka, H., Obata, F., Matsubara, T., Mizumoto, H., 1994, Active Chatter Suppression of Slender Boring Bar Using Piezoelectric Actuators. JSME international journal. Ser. C, Dynamics, control, robotics, design and manufacturing, 37/3: 601–606. https://doi.org/10.1299/jsmec1993.37.601.
[17] Wang, M., Fei, R., 1999, Chatter Suppression Based on Nonlinear Vibration Characteristic of Electrorheological Fluids. International Journal of Machine Tools and Manufacture, 39/12: 1925–1934. https://doi.org/10.1016/S0890-6955(99)00039-5.
[18] Lu, X., Chen, F., Altintas, Y., 2014, Magnetic Actuator for Active Damping of Boring Bars. CIRP Annals, 63/1: 369–372. https://doi.org/10.1016/J.CIRP.2014.03.127.
[19] Tewani, S.G., Rouch, K.E., Walcott, B.L., 1995, A Study of Cutting Process Stability of a Boring Bar with Active Dynamic Absorber. International Journal of Machine Tools and Manufacture, 35/1: 91–108.
[20] Abele, E., Haydn, M., Grosch, T., 2016, Adaptronic Approach for Modular Long Projecting Boring Tools. CIRP Annals, 65/1: 393–396.
[21] Munoa, J., Sanz-Calle, M., Dombovari, Z., Iglesias, A., Pena-Barrio, J., Stepan, G., 2020, Tuneable Clamping Table for Chatter Avoidance in Thin-walled Part Milling. CIRP Annals, 69/1: 313–316. https://doi.org/10.1016/j.cirp.2020.04.081.
[22] Rivin, E.I., 1999, Stiffness and Damping in Mechanical Design. Marcel Dekker, New York.
[23] Duncan, G.S., Tummond, M.F., Schmitz, T.L., 2005, An Investigation of the Dynamic Absorber Effect in High-speed Machining. International Journal of Machine Tools and Manufacture, 45/4–5: 497–507. https://doi.org/10.1016/j.ijmachtools.2004.09.005.
[24] Houck, L., Schmitz, T.L., Scott Smith, K., 2011, A Tuned Holder for Increased Boring Bar Dynamic Stiffness. Journal of Manufacturing Processes, 13/1: 24–29. https://doi.org/10.1016/J.JMAPRO.2010.09.002.
[25] Schmitz, T.L., Donalson, R.R., 2000, Predicting High-speed Machining Dynamics by Substructure Analysis. Cirp Annals, 49/1: 303–308.
[26] Mohammadi, Y., Azvar, M., Budak, E., 2018, Suppressing Vibration Modes of Spindle-holder-tool Assembly Through FRF Modification for Enhanced Chatter Stability. CIRP Annals, 67/1: 397–400. https://doi.org/10.1016/j.cirp.2018.03.003.
[27] Sanz-Calle, M., Dombovari, Z., Munoa, J., Iglesias, A., López de Lacalle, L.N., 2021, Self-Tuning Algorithm for Tuneable Clamping Table for Chatter Suppression in Blade Recontouring. Applied Sciences, 11/6: 2569. https://doi.org/10.3390/APP11062569.
[28] Park, S.S., Altintas, Y., Movahhedy, M., 2003, Receptance Coupling for End Mills. International Journal of Machine Tools and Manufacture, 43/9: 889–896. https://doi.org/10.1016/S0890-6955(03)00088-9.
[29] Mancisidor, I., Urkiola, A., Barcena, R., Munoa, J., Dombovari, Z., Zatarain, M., 2014, Receptance Coupling for Tool Point Dynamic Prediction by Fixed Boundaries Approach. International Journal of Machine Tools and Manufacture, 78:18–29. https://doi.org/10.1016/J.IJMACHTOOLS.2013.12.002.
[30] Magyar, B., Wohlfart, R., Zana, R., Hénap, G., Csernák, G., Stepan, G., 2020, Evaluation of Contact Force Distribution Along A Curve, Based on Measured Electric Potentials. Acta Mechanica 232:3, 232/3: 853–879. https://doi.org/10.1007/S00707-020-02898-Y.
[31] Han, S.M., Benaroya, H., Wei, T., 1999, Dynamics of Transversely Vibrating Beams Using Four Engineering Theories. Journal of Sound and Vibration, 225/5: 935–988.
[32] Timoshenko, S., 1976, Strength of Materials - Part 1. Krieger Pub Co., Florida.
[33] Altintas, Y., Eynian, M., Onozuka, H., 2008, Identification of Dynamic Cutting Force Coefficients and Chatter Stability with Process Damping. CIRP Annals, 57/1: 371–374.
[34] Ahmadi, K., Ismail, F., 2011, Analytical Stability Lobes Including Nonlinear Process Damping Effect on Machining Chatter. International Journal of Machine Tools and Manufacture, 51/4: 296–308.

[35] Budak, E., Tunc, L.T., 2010, Identification and Modeling of Process Damping in Turning and Milling Using a New Approach. CIRP Annals, 59/1: 403–408.
[36] Altintas, Y., 2012, Manufacturing Automation. 2nd ed. Cambridge University Press, Cambridge, UK.
[37] Colwell, L., 1954, Predicting the Angle of Chip Flow For Single-point Cutting Tools. Transactions of the ASME, 76:199.
[38] Insperger, T., Stépán, G., 2002, Semi-discretization Method for Delayed Systems. International Journal for Numerical Methods in Engineering, 55/5: 503–518.
[39] Richardson M.H., Formenti D.L., 1982. Parameter Estimation From Frequency Response Measurements Using Rational Fraction Polynomials. Proceedings of the International Modal Analysis Conference & Exhibit. Union College Schenectady, NY 167–181.
[40] Cauberghe B., Guillaume P., Verboven P., Parloo E., Vanlanduit S., 2004. The secret behind clear stabilization diagrams: the influence of the parameter constraint on the stability of the poles. Proceedings of the 10th SEM international congress & exposition on experimental and applied mechanics 7.
[41] Dombovari, Z., 2021, Stability Properties of Regenerative Cutting Processes, Based on Impulse Response Functions Expressed in the Impulse Dynamic Subspace. International Journal of Machine Tools and Manufacture, 162:103691https://doi.org/10.1016/J.IJMACHTOOLS.2021.103691.